# Orbital moments of $CrO_2$ and $Fe_3O_4$ studied by MCD in soft X-ray absorption

D.J. Huang [a,b,*], C.F. Chang [a], J. Chen [c], H.-J. Lin [a], S.C. Chung [a], H.-T. Jeng [d],
G.Y. Guo [a,e], W.B. Wu [a,b], S.G. Shyu [f,g], C.T. Chen [a]

[a] *National Synchrotron Radiation Research Center, Hsinchu 300, Taiwan, ROC*
[b] *Department of Electrophysics, National Chiao-Tung University, Hsinchu 300, Taiwan, ROC*
[c] *Department of Physics, National Chung Cheng University, Chia-Yi 621, Taiwan, ROC*
[d] *Physics Division, National Center for Theoretical Sciences, Hinchu 300, Taiwan, ROC*
[e] *Department of Physics, National Taiwan University, Taipei 106, Taiwan, ROC*
[f] *Institute of Chemistry, Academia Sinica, Nankang, Taipei 115, Taiwan, ROC*
[g] *Department of Chemistry, National Central University, Tao-Yuan 320, Taiwan, ROC*

Available online 2 April 2004

## Abstract

We present studies of orbital magnetic moments of $CrO_2$ and $Fe_3O_4$ by measuring magnetic circular dichroism (MCD) in soft X-ray absorption. The results show that $Fe_3O_4$ exhibits large orbital moments, as a consequence of the strong Coulomb interactions of Fe 3d electrons. In contrast, orbital moments of Cr in $CrO_2$ are nearly quenched, revealing that Cr 3d electrons are strongly hybridized with O 2p electrons and more delocalized as compared with those of Fe in $Fe_3O_4$. Comparing the MCD data with the band structure calculations based on local spin density approximation with on-site Coulomb energy $U$ taken into account, we conclude that to include the on-site Coulomb interactions of 3d electrons is essential for adequately describing the electronic structure of $CrO_2$ and $Fe_3O_4$.
© 2004 Elsevier B.V. All rights reserved.

## 1. Introduction

Transition metal oxides, which are interesting for fundamental research and important for technological applications, exhibit anomalous and interesting physical properties [1]. These interesting properties are determined by the coupling between charge, orbital characters and spin of valence electrons, and the lattice degrees of freedom in transition-metal oxides. For instance, magnetic oxides such as $Fe_3O_4$, manganates and $CrO_2$ have drawn much attention because of metal-to-insulator transition, colossal magnetoresistance, and half-metallic behavior.

Orbital magnetism is closely related to many novel phenomena, such as magneto-optical effect, magnetostriction, and magnetocrystalline anisotropy. Orbital magnetic moments of 3d transition metals are generally quenched because of crystal field. Some 3d transition metal oxides exhibit large unquenched orbital magnetic moments, which arises mainly from spin-orbit interaction in the localized 3d orbital whereby the atomic field is deformed in a relatively slight manner by the crystal field. In addition, strong Coulomb repulsion of 3d electrons localizes 3d orbitals and reduces the ligand field on the metal atoms, leading to large unquenched orbital moments [2,3]. For instance, results of magnetic X-ray scattering indicate that the orbital magnetic moment of NiO is rather large [4].

Measurements of orbital moments provide us with an opportunity to explore the localized nature of 3d electrons in transition metal oxides [2,3]. Several experimental techniques, such as neutron scattering, magnetic X-ray scattering, and magnetic circular dichroism (MCD) in X-ray absorption spectroscopy (XAS) are useful in studying orbital moments. Element-specific separation of spin and orbital magnetization can be achieved by MCD in X-ray

---

absorption through the MCD sum rules, which specify the relation of spin and orbital moments to integrated XAS and integrated MCD spectra [5–10]. For example, the orbital and spin magnetic moments of Fe and Co obtained on applying the MCD sum rules to high resolution $L_{2,3}$-edge XAS and MCD data agree well with those obtained from Einstein-de Haas gyromagnetic ratio measurements [9]. Direct transmission is the most reliable method to obtain accurate orbital magnetic moments [9], but this method is technically inapplicable to epitaxial thin films or single crystals. However indirect X-ray absorption measurement techniques, like the total electron yield (TEY) method for some transition metals, suffer typically from saturation and self-absorption effects that can produce inaccurate values of orbital magnetic moment. To correct indirect XAS measurements for saturation and self-absorption effects is particularly crucial in measuring orbital moments [11].

Half-metallic oxides such as $CrO_2$ have recently drawn renewed attention due to their interesting magnetic and electrical properties. These properties are potentially important for future spintronics which takes full advantage of electrons' spins as well as their charge in information circuits. In a half-metallic material [12], one spin channel is conductive, but the other spin channel is insulating. Based on band structure calculations, many materials have been predicted to be half-metallic. However, experiments performed on some predicted half-metals do not show 100% spin polarization of the conduction electrons. One of the main reasons is that electron correlation effects prevent the conduction electrons from being 100% spin polarized. One therefore can measure orbital moments to explore the localized nature of 3d electrons in half-metallic oxides [2,3]. For instance, examining whether orbital moments are quenched is important in revealing the electronic nature of $Fe_3O_4$.

In this paper, we present measurements of MCD in soft X-ray absorption to study orbital magnetic moments of $CrO_2$ and $Fe_3O_4$. MCD in X-ray absorption spectroscopy were performed with correction for saturation effects. We also compare measurements of orbital moments with band structure calculations based on local spin density approximation with on-site Coulomb energy $U$ taken into account (LDA + $U$).

The rest of this paper is organized as follows. In the next section, we briefly describe the experimental methods including MCD methods and epitaxial growth of $CrO_2$ and $Fe_3O_4$ thin films. Results and discussion of MCD measurements are presented in Section 3, followed by the conclusions.

## 2. Experimental

### 2.1. Epitaxial CrO₂ and Fe₃O₄ thin films

Epitaxial $CrO_2$ films were grown on $TiO_2(1\,0\,0)$ substrates by chemical vapor deposition (CVD) [13]. The substrates were ultrasonically cleaned with acetone, 1,1,1-trichloroethane, 10% hydrofluoric acid and distilled water before air-drying. The deposition was at 400 °C by using $CrO_3$ as the precursor. X-ray diffraction results reveal that $CrO_2$ films are single crystalline and epitaxial; measurements of magneto-optical Kerr effect show a square magnetic hysteresis loop, indicating high magnetic remanence of $CrO_2$ films.

Thin films of $Fe_3O_4$ were grown on MgO(0 0 1) single crystals which provide an ideal template for epitaxial growth. The lattice constant of $Fe_3O_4$, 8.396 Å, is close to twice of the MgO lattice constant, 4.211 Å, resulting in an epitaxial growth with a small lattice mismatch. Both the rocksalt structure of MgO and the inverse spinel structure of $Fe_3O_4$ are based on a f.c.c. oxygen anion lattice, allowing a continuation of the oxygen sublattice over the MgO/$Fe_3O_4$ interface. We achieved to grow epitaxial 100-monolayer (ML) (i.e. 210 Å thick) $Fe_3O_4$ thin films with evaporating Fe from an effusion cell at the presence of oxygen. Before film growth, the MgO(1 0 0) substrate was cleaved ex situ and annealed at a temperature around 650 °C with an oxygen pressure of $5 \times 10^{-8}$ Torr for 1–2 h to remove contamination such as hydrocarbons. The cleanliness and the structure of MgO(1 0 0) surface were characterized by photoemission and reflection high energy electron diffraction (RHEED), respectively. The growth rate of $Fe_3O_4$ thin films was ~1 ML per minute. Structure of the thin films was real-time monitored by RHEED and its thickness was calibrated with the intensity oscillation of the RHEED specular beam, as shown in Fig. 1(a). The results reveal that the growth of $Fe_3O_4$ thin films on MgO(0 0 1) is in an epitaxial layer-by-layer mode. The film and its epitaxy were fully characterized by X-ray diffraction. The composition of the film was examined by core-level photoemission and $L$-edge X-ray absorption of Fe; the results are identical to those obtained from $Fe_3O_4$ single crystals. In addition, the resistance measurement shown in Fig. 1(b) reveals that our film has a well-defined Verwey transition temperature which is also a good indication of the quality of our $Fe_3O_4$ thin films.

### 2.2. MCD sum rules

The sum rules of MCD in X-ray absorption permit element-selective separation of spin and orbital contributions to the total magnetic moment of materials [5,6,9,8,10]. Calculations on the basis of a tight-binding approximation show that $K$-edge MCD spectra is generated mainly by the 3d orbital moment on the neighboring sites through the p–d hybridization [14]. MCD spectra of an s-level absorption reflect the p-projected orbital magnetization density of unoccupied states. According to X-ray MCD sum rules, orbital magnetic moments $m_{orb}$ in units of $\mu_B$ per atom can be obtained from $K$-edge XAS and MCD spectra. Sum rules of $K$-edge absorption relate orbital magnetic moments to $K$-edge XAS and MCD spectra as
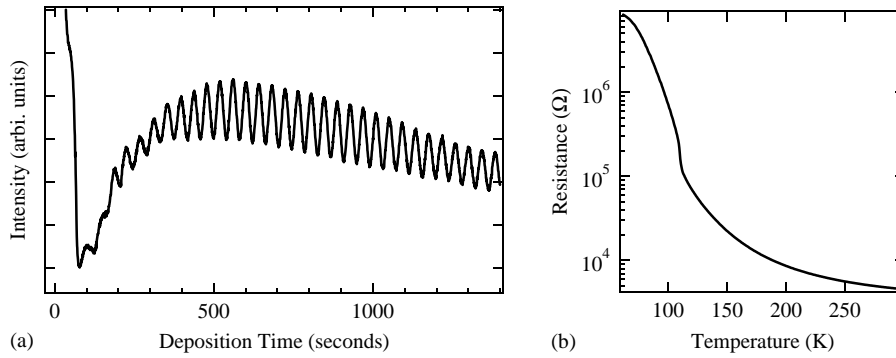
Fig. 1. (a) Intensity oscillation of RHEED specular beam and (b) temperature dependence of resistance measurement of 100 ML $Fe_3O_4$ thin films grown on MgO(1 0 0).

[5,7,8]:

$$m_{orb} = -\frac{2}{3}\frac{\int_K (\sigma_+ - \sigma_-)\,d\omega}{\int_K (\sigma_+ + \sigma_-)\,d\omega}(6 - n_p), \qquad (1)$$

where $n_p$ and $\omega$ are the electron occupation number in the 2p states and the photon energy, respectively; $\sigma_+$ and $\sigma_-$ are cross sections for absorption taken with the projection of the spin of the incident photons parallel and anti-parallel to the spin of the majority electrons in transition metals, respectively. K denotes the integration range across the K-edge of the spectra.

With X-ray MCD sum rules, $L_{2,3}$-edge XAS and MCD spectra also provide information on the orbital $m_{orb}$ and spin $m_{spin}$ magnetic moments of transition metals as in the following equations:

$$m_{orb} = -\frac{4}{3}\frac{\int_{L_{2,3}} (\sigma_+ - \sigma_-)\,d\omega}{\int_{L_{2,3}} (\sigma_+ + \sigma_-)\,d\omega}(10 - n_d), \qquad (2)$$

and

$$m_{spin} + 7\langle T_z \rangle = -\frac{6\int_{L_3}(\sigma_+ - \sigma_-)\,d\omega - 4\int_{L_{2,3}}(\sigma_+ - \sigma_-)\,d\omega}{\int_{L_{2,3}}(\sigma_+ + \sigma_-)\,d\omega} \times (10 - n_d), \qquad (3)$$

where $n_d$ is the 3d electron occupation number of transition metals. $L_{2,3}$ denotes the integration range across $L_2$ and $L_3$ absorption edges. $\langle T_z \rangle$ is the expectation value of magnetic dipole operator. For cubic materials, $\langle T_z \rangle$ is typically negligible. Thus the ratio $m_{orb}/m_{orb}$ of orbital to spin moments can be expressed as

$$\frac{m_{orb}}{m_{spin}} \approx \frac{2\int_{L_3+L_2}(\sigma_+ - \sigma_-)\,d\omega}{9\int_{L_3}(\sigma_+ - \sigma_-)\,d\omega - 6\int_{L_3+L_2}(\sigma_+ - \sigma_-)\,d\omega}. \qquad (4)$$

With Eq. (4), MCD spectra provide us with a measurement of $m_{orb}/m_{spin}$, requiring no information on the background of XAS spectra, the average number of 3d holes, and the degree of circular polarization of incident photons.

## 2.3. MCD measurements

We carried out MCD measurements in soft X-ray absorption with the elliptically polarized undulator (EPU) beamline [15,16] and the Dragon beamline of the National Synchrotron Radiation Research Center in Taiwan. The EPU can generate circularly polarized light or linearly polarized light with the polarization in the horizontal or vertical direction with respect to the storage ring. The Dragon beamline delivers circularly polarized light via a bending magnet. All soft X-ray absorption measurements were taken with photons of an energy resolution 0.2 eV. The incident angle was 45° off the sample normal. During the measurements, the thin films were at the magnetically remanent state and kept at a temperature of 80 K. Sample drain current was detected as the absorption signal.

For measuring L-edge XAS of Fe with the TEY method, there exists significant saturation effects. To extract the correct value of orbital moments by applying the sum rules to the MCD data obtained with a TEY measurement, one needs to examine carefully the saturation effects. When saturation occurs, the measured TEY signal is no longer uniformly proportional to the absorption cross section, leading to an inaccurate measurement of orbital magnetic moments [11]. The degree to which saturation occurs in the TEY signal depends on the relative photon penetration depth $\lambda_x$ and electron sampling depth $\lambda_e$. The measured absorption signal $I_{TEY}$ in a TEY measurement is reduced by a correction factor $f = 1/(1 + \lambda_e/\lambda_x \cos\theta)$, where $\theta$ is the incidence angle of X-ray with respect to the surface normal [11], i.e., $I_{TEY} = fC\sigma$, in which $C$ and $\sigma$ are a proportion constant and the absorption cross section, respectively. The $\lambda_e$ of $Fe_3O_4$ was estimated to be 50 Å, and $\lambda_x$ at the $L_3$ and $L_2$ edges, respectively, were 170 and 525 Å [21]. One thus would expect to have 37 and 16% reduction in the TEY signal of $Fe_3O_4$ at the $L_3$ and $L_2$ peaks, respectively, if the saturation effects were not corrected.

To determine the energy-dependent correction factor $f$ of $Fe_3O_4$, we measured the energy-dependent X-ray penetration depth $\lambda_x$ with a new quasi-transmission technique in XAS. The underlying concept of this technique is shown in
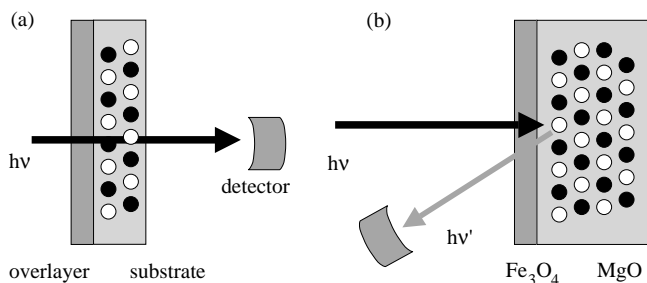
Fig. 2. Schematic diagrams of (a) direct transmission and (b) quasi-transmission for soft X-ray absorption measurements. Filled and open circles shown in the substrate represent the composition atoms Mg and O, respectively. In quasi-transmission, O fluorescence $h\nu'$ from the substrate is detected.

Fig. 2. For incident photons with energy $h\nu$ greater than the energy of O $K$-edge fluorescence, the transmitted photons through the $Fe_3O_4$ overlayer stimulate O $K$-edge fluorescence $h\nu'$ from the substrate MgO. The dependence of O $h\nu'$ intensity on the incident photon energy accordingly provides an avenue for detecting relatively the transmitted photon intensity. The O atoms in substrate MgO can serve as detectors for transmission measurement of XAS. The contribution of O fluorescence from the $Fe_3O_4$ overlayer is negligible as compared to that from the substrate, since the penetration depth of O fluorescence is much larger than the thickness of $Fe_3O_4$ overlayer. A plot of O $K$-edge fluorescence $h\nu'$ intensity versus incident photon energy $h\nu$ in the region of the Fe $L$-edge absorption therefore gives rise to a measurement of transmission spectrum for Fe $L$-edge absorption of $Fe_3O_4$ overlayer.

The validity of this quasi-transmission technique was examined by measuring the X-ray penetration depth of 80 Å thick pure Fe thin films in the region of the $L_{2,3}$-edge absorption, as shown in Fig. 3. A semiconductor fluorescence

detector was used to measure the intensity of O $K$-edge fluorescence. Our measured $\lambda_x$ of Fe thin film is in good agreement with that of previous direct transmission results [9,11]. These test results establish unambiguously that a quasi-transmission measurement is as accurate as a direct transmission measurement in obtaining X-ray penetration depth $\lambda_x$ of Fe.

## 3. Results and discussion

### 3.1. Orbital moments of $CrO_2$

Fig. 4 presents the O $K$-edge XAS and MCD of $CrO_2$ [17]. After correction for the incomplete polarization and the incident angle of soft X-ray, i.e. multiplying $(\sigma_+ - \sigma_-)$ by $1/[\cos 45° \times 0.6]$ for MCD spectra while keeping XAS$=(\sigma_+ + \sigma_-)$ unchanged, we found that the MCD to XAS ratio at the pre-peak position of O $K$-edge absorption is 4.1%, which is larger than that, 3%, observed on $La_{1-x}Sr_xMnO_3$ single crystals [18]. For $q$ and $r$ as the integrated intensities of MCD and XAS spectra across the
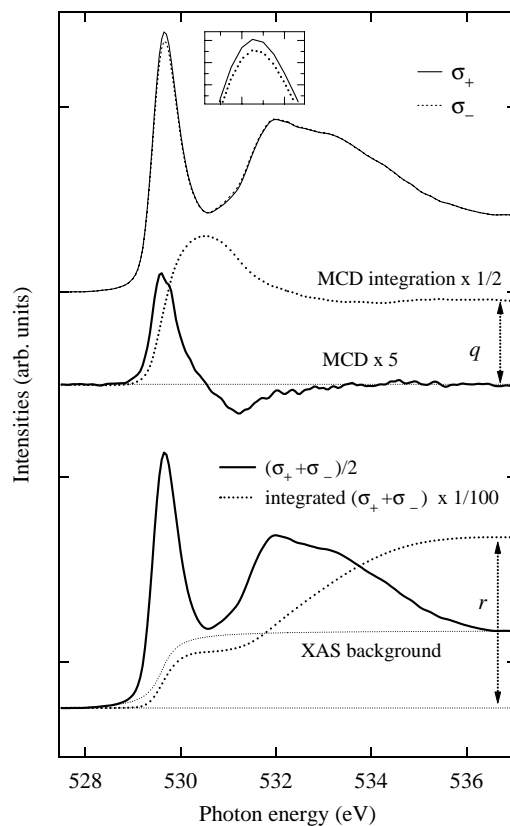


Fig. 4. $K$-edge XAS and MCD spectra of O in $CrO_2$ (after [17]). *Top*: XAS spectra with spin of photons parallel (denoted as $\sigma_+$) and anti-parallel (denoted as $\sigma_-$) to that of Cr 3d majority electrons, respectively; *middle*: MCD, i.e. $(\sigma_+ - \sigma_-)/[\cos 45° \times 0.6]$, and MCD integration of the O $K$-edge absorption; *bottom*: XAS integration spectra with an XAS background (thin broken line). The $r$ and $q$ denote the integration of XAS and MCD spectra across the $K$-edge, respectively.



Fig. 3. (a) $L_{2,3}$-edge quasi-transmission measurements and (b) average X-ray penetration depth $\lambda_x$ of 80 Å thick pure Fe thin films grown on MgO(0 0 1). $\sigma_+$ and $\sigma_-$ are defined in the text.

$K$-edge, the orbital magnetic moment per O atom is $m_{\text{orb}} = -(2/3)(q/r)(6-n_{\text{p}})$. To quantitatively obtain the O 2p hole density, we compared the spectrum of O 1s XAS of $CrO_2$ with that of $O_2$ molecules. The average number of O 2p holes per atom in $CrO_2$ is estimated to be 0.5 [17]. With an arctangent-like edge-jump function for the background of the XAS spectra, the O orbital magnetic moment is therefore estimated to be $-(0.003 \pm 0.001)\mu_{\text{B}}$. The large uncertainty originates mainly from our estimate of the number of O 2p holes, the background functions of XAS spectra, and the uncertainty from the degree of circular polarization of incident photons.

Fig. 5 displays the Cr L-edge XAS and MCD spectra of $CrO_2$ [17]. For $q$ and $r$ as the integrated intensities of MCD and XAS spectra across the $L_{2,3}$ edges, respectively, as shown in Fig. 5, the orbital magnetic moment of Cr is $m_{\text{orb}} = -(4/3)(q/r)(10-n_{\text{d}})$. With an appropriate arctangent-like edge-jump function for the XAS background and $n_{\text{d}} \sim 1$, our MCD data indicate that the orbital magnetic moment of Cr is $-(0.06 \pm 0.02)\mu_{\text{B}}$ [17]. Unlike the case of $Fe_3O_4$, MCD data of $CrO_2$ are not severely affected by saturation effects, because the difference in intensity between absorption at the Cr $L_3$ and $L_2$ edges is significantly smaller than that of Fe. In our MCD measurements on $CrO_2$, saturation effects have been corrected by normalizing the XAS spectra to the normal incidence data. In contrast, our MCD and XAS data do not provide quantitatively information on the spin moment of Cr because one can not uniquely define which part of the spectra belongs to the $L_3$ or the $L_2$ edges. This is due to the large multiplet splitting in the XAS final states relative to the Cr 2p core-level spin-orbit splitting. Nevertheless, the integration spectrum of our MCD data indicates that the orbital moment of Cr is opposite to its spin moment [17].

MCD measurements presented above, nevertheless, provide valuable qualitative information on element specific orbital magnetic moment. Our measurements reveal that Cr orbital moments of $CrO_2$ is opposite to its spin moment, but parallel aligned to O orbital moment. We found that the measured Cr orbital moment of $-(0.06 \pm 0.02)\mu_{\text{B}}$ is consistent with those of LDA + U calculations with $U = 3$–4 eV [17,19].

### 3.2. Orbital moments of $Fe_3O_4$

Fig. 6 shows Fe $L_{2,3}$-edge XAS and MCD spectra of $Fe_3O_4$ thin films obtained with TEY measurements. Before obtaining the orbital moments, we first discuss the multiplet structure of the spectra. The 2p XAS spectrum reflects directly the nature of the 3d electronic ground state. The local ground state of Fe ions is a mixture of configurations $3d^n$, $3d^{n+1}\underline{L}$, and $3d^{n+2}\underline{L}^2$ with $n = 5$ and 6 for $Fe^{3+}$ and $Fe^{2+}$ ions, respectively, where $\underline{L}$ denotes a ligand hole. The final state in $L$-edge absorption is predominantly a mixture of configurations $\underline{2p}3d^{n+1}$ and $\underline{2p}3d^{n+2}\underline{L}$. The $\underline{2p}3d^{n+1}$ configuration exhibits multiplet structure as a consequence of the 2p–3d exchange interaction, whereas
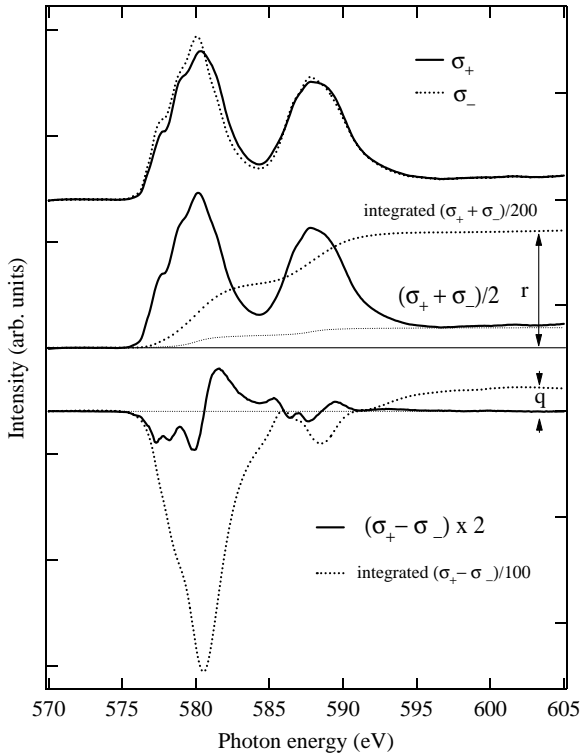


Fig. 5. $L_{2,3}$-edge XAS and MCD spectra of Cr in $CrO_2$ (after [17]). *Top*: XAS spectra with incident photon of different spin directions; *middle*: XAS integration spectra with an arctangent-like edge-jump function of background (thin broken line); *bottom*: MCD and MCD integration spectra. The descriptions of the figure correspond to those of Fig. 4.
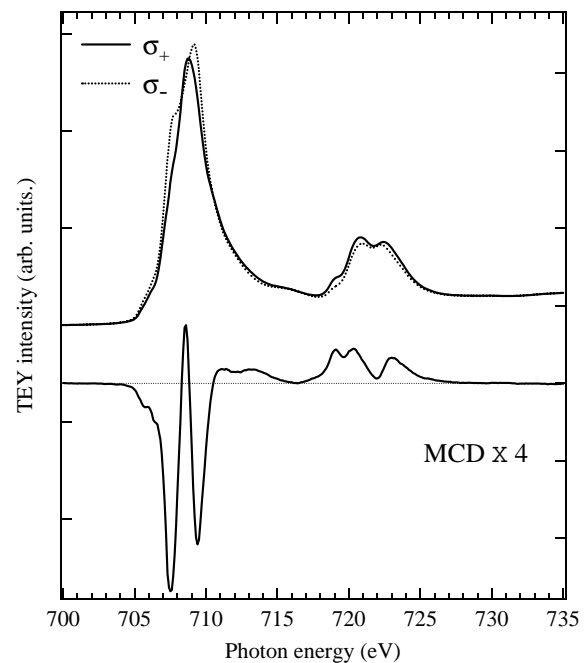


Fig. 6. Fe $L_{2,3}$-edge XAS and MCD spectra of $Fe_3O_4$ thin films obtained with TEY measurements. $\sigma_+$ and $\sigma_-$ are defined in the text.
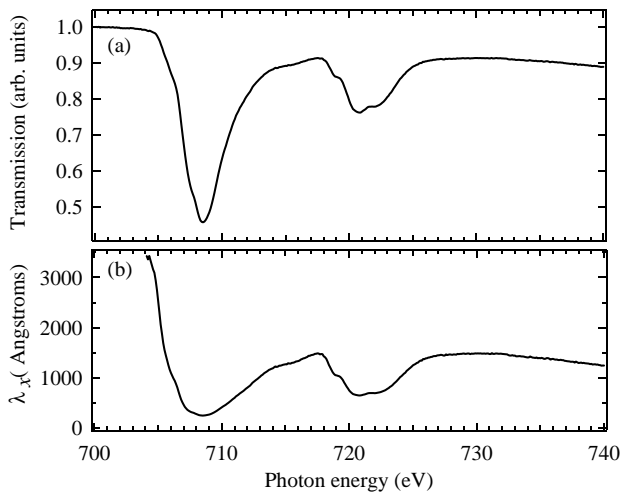
Fig. 7. Fe $L_{2,3}$-edge X-ray absorption in quasi-transmission mode (a) and penetration depth $\lambda_x$ (b) of $Fe_3O_4$ taken with quasi-transmission measurements.



Fig. 8. Fe $L_{2,3}$-edge MCD and MCD integration of $Fe_3O_4$ obtained from TEY measurements. The solid and dash lines are with and without correction for saturation effects, respectively. $p$ and $q$ denote the integrals of the MCD spectrum across the $L_3$ and the $L_{2,3}$ absorption edges, respectively.

a broad band feature exists in the configuration $2p3d^{n+2}\underline{L}$ resulting from the bandlike character of the ligand hole. The MCD measurements suggest that the leading edge of the $L_3$ absorption (i.e. at photon energy 707.5 eV) with a negative MCD peak results mainly from $2p \rightarrow 3d$ transition in the B-site $Fe^{2+}$ ions. Another negative MCD peak at photon energy 709.4 eV is derived predominately from the B-site $Fe^{3+}$ ions. The energy difference between these two MCD peaks is $\sim(U_{dd} - U_{dc})$, where $U_{dd}$ and $U_{dc}$ are the Coulomb interaction energies between 3d electrons and between 3d electrons and 2p core holes, respectively. In addition, the positive MCD peak at photon energy 708.6 eV predominantly results from the A-site $Fe^{3+}$ ions.

To extract the correct value of orbital moments by applying the sum rules to these MCD data, we have obtained the correction factor for saturation effects of Fe L-edge XAS measurements by the measuring X-ray absorption length. Fig. 7(a) shows the quasi-transmission measurements on Fe $L_{2,3}$-edge XAS of epitaxial $Fe_3O_4$ thin films of thickness 100 ML at 300 K. These quasi-transmission data give rise to a measurement on the X-ray penetration depth $\lambda_x$ of $Fe_3O_4$, as shown in Fig. (b), in which $\lambda_x$ at the $L_3$ and $L_2$ absorption peaks are similar to those shown in [21]. With the measured $\lambda_x$ and the electron sampling depth $\lambda_e = 50$ Å from [21], we achieved to have MCD measurements on $Fe_3O_4$ with correction for saturation effects, as shown in Fig. 8. There is a pronounced difference ($\sim$20%) between the $L_3$ MCD spectra with and without correction for saturation effects, whereas the difference in the $L_2$ MCD is relatively small. For $p$ and $q$ as the integrals of the MCD spectrum across the $L_3$ and the $L_{2,3}$ absorption edges, respectively, $m_{orb}/m_{spin}$ is $2q/(9p - 6q)$. We found that $m_{orb}/m_{spin}$ of $Fe_3O_4$ per formula unit are 0.21 and 0.17 with and without correction for saturation effects, respectively, if the $7\langle T_z \rangle$ contribution is neglected.
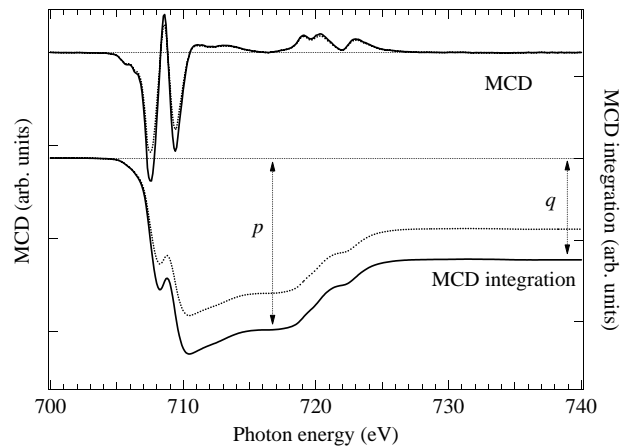
$LSDA + U$ calculations show the values of spin moment and magnetic dipole moments of $Fe_3O_4$ are, respectively, $3.97\mu_B$ and $0.155\mu_B$ per formula unit [20]. The contribution of $7\langle T_z \rangle$ thus gives rise to 4% of increase in the $m_{orb}/m_{spin}$ ratio. Therefore, we conclude that $m_{orb}/m_{spin}$ of $Fe_3O_4$ per formula unit is $0.22 \pm 0.04$, suggesting an average orbital magnetic moment of $(0.44 \pm 0.08)\mu_B$ per B-site Fe atom. To unravel the origin of the unquenched orbital magnetic moments of $Fe_3O_4$, we resort to configuration interaction approach for the ground state electronic configuration of the octahedral $Fe^{2+}$ ions based on a $FeO_6$ cluster model. We calculated the occupation probabilities of down-spin 3d electrons of high-spin $Fe^{2+}$ ions in an octahedral crystal field. With the spin-orbit interaction, but without the crystal field and the hybridization between Fe 3d and O 2p, the orbital moment of $Fe^{2+}$ ions maximizes, i.e., $m_{orb} = 2\mu_B$ as expected from the Hund's coupling. If the the crystal field and the hybridization are included, the dominant down-spin $t_{2g}$ state of $Fe^{2+}$ is $1/\sqrt{2}(Id_{yz} + d_{zx})$, leading to an orbital moment of $1\mu_B$ [22], i.e., average $0.5\mu_B$ per B-site Fe atom in $Fe_3O_4$. Our MCD measurements thus indicate that 3d electrons of B-site Fe in $Fe_3O_4$ are with a strong localized nature even at temperature above the Verwey transition.

## 4. Conclusions

We have studied orbital magnetic moments of $CrO_2$ and $Fe_3O_4$ by measuring MCD in soft X-ray absorption. The results show that orbital moments of Cr in $CrO_2$ are are nearly quenched, revealing that Cr 3d electrons are strongly hybridized with O 2p electrons and more delocalized as compared with those of Fe in $Fe_3O_4$. We found that oxygen atoms in $CrO_2$ exhibit a significant orbital magnetic moment compared to those of other oxides. Orbital moments of O in

$CrO_2$ are parallel coupled to that of Cr, while the spin moments are anti-parallel coupled. In addition, the magnitudes of spin and orbital moments of Cr are enhanced as on-site Cr 3d–3d Coulomb interaction increases. We also found that $Fe_3O_4$ exhibits large orbital moments, in contrast to nearly quenched orbital moments of Cr in $CrO_2$. Large orbital polarization of Fe in $Fe_3O_4$ caused by on-site Coulomb interactions of 3d electrons results in unquenched orbital moments of $Fe_3O_4$. As compared with LDA $+ U$ calculations, our results indicate that one has to properly include on-site Coulomb interactions of 3d electrons in $CrO_2$ and $Fe_3O_4$ in order to describe their electronic structure adequately.

## Acknowledgements

## References

[1] M. Imada, A. Fujimori, Y. Tokura, Rev. of Modern Phys. 70 (1998) 1039.

[2] I.V. Solovyev, A.I. Liechtenstein, K. Terakura, Phys. Rev. Lett. 80 (1998) 5758.

[3] S.K. Kwon, B.I. Min, Phys. Rev. B 62 (2000) 73.

[4] V. Fernandez, C. Vettier, F. de Bergevin, C. Giles, W. Neubeck, Phys. Rev. B 57 (1998) 7870.

[5] B.T. Thole, P. Carra, F. Sette, G. van der Laan, Phys. Rev. Lett. 68 (1992) 1943.

[6] P. Carra, B.T. Thole, M. Altarelli, X. Wang, Phys. Rev. Lett. 70 (1993) 694.

[7] A. Ankudinov, J. J. Rehr, Phys. Rev. B 51 (1995) 1282.

[8] G.Y. Guo, Phys. Rev. B 57 (1998) 10295.

[9] C.T. Chen, Y.U. Idzerda, H.-J. Lin, N.V. Smith, G. Meigs, E. Chaban, G.H. Ho, E. Pellegrin, F. Sette, Phys. Rev. Lett. 75 (1995) 152.

[10] R. Wu, A.J. Freeman, Phys. Rev. Lett. 73 (1994) 1994.

[11] R. Nakajima, J. Stohr, Y.U. Idzerda, Phys. Rev. B 59 (1999) 6421.

[12] R.A. de Groot, F.M. Mueller, P.G. van Engen, K.H.J. Buschow, Phys. Rev. Lett. 50 (1983) 2024.

[13] X.W. Li, A. Gupta, G. Xiao, Appl. Phys. Lett. 75 (1999) 713.

[14] J. Igarashi, K. Hirai, Phys. Rev. B 50 (1994) 17820.

[15] C.S. Hwang, S. Yeh, Nucl. Instr. and Meth. A420 (1999) 29.

[16] S.-C. Chung, J. Chen, L.-R. Huang, R.T. Wu, C.-C. Chen, N.-F. Cheng, J.M. Chuang, P.-C. Tseng, D.J. Huang, C.F. Chang, S.-Y. Perng, C.T. Chen, K.-L. Tsang, Nucl. Instr. and Meth. A 467–478 (2001) 445.

[17] H.-T. Huang, H.-T. Jeng, C.-F. Chang, G.Y. Guo, J. Chen, W.P. Wu, S.C. Chung, S.G. Shyu, C.C. Wu, C.T. Chen, Phys. Rev. B 66 (2002) 174440.

[18] E. Pellegrin, H.J. Tjeng, F.M. de Groot, R. Hesper, G.A. Sawatzky, Y. Moritomo, Y. Tokura, J. Electron. Spectrosc. Relat. Phenom. 86 (1997) 115.

[19] H.T. Jeng, G.Y. Guo, J. Appl. Phys. 92 (2002) 951.

[20] H.-T. Jeng, et al., manuscript in preperation.

[21] S. Gota, M. Gautier-Soyer, M. Sacchi, Phys. Rev. B 62 (2000) 4187.

[22] T. Jo, T. Shishidou, J. Phys. Soc. Jpn. 67 (1998) 2505.